Journal of Naval Architecture and Marine Engineering
December, 2021
http://dx.doi.org/10.3329/jname.v18i2.53624 *http://www.banglajol.info*

EFFECT OF ANEURYSMATIC ARTERY ON BLOOD FLOW HAVING PERMEABILITY IN HUMAN ORGAN

Mohammed Nasir Uddin[*1], Md. Abdul Alim[2], Md. Mashud Karim[2], M. M. Alam[3]

[1]Department of Information and Communication Technology (ICT), Bangladesh University of Professionals (BUP), Dhaka-1216, Bangladesh, [*]Email: nasirbuet@gmail, com

[2]Department of Mathematics, Bangladesh University of Engineering and Technology (BUET), Dhaka, Bangladesh Email: maalim@math.buet.ac.bd

[2]Department of *naval architecture and marine engineering*, Bangladesh University of Engineering and Technology (BUET), Dhaka, Bangladesh, Email: mmkarim@name.buet.ac.bd.

[3]Dept. of Electrical and Electronic Engineering, Islamic University, Kushtia-7003, Bangladesh, Email: malam@eee.iu.ac.bd

Abstract:

Blood flow in a double aneurysmatic artery of the normal tissue is studied. A Finite element method is used to analyze numerical simulation of blood flow through aneurysmatic arteries and Comsol multiphysics software is used for blood flow simulation. The Newtonian, generalized Newtonian, Oldroyd-B, and generalized Oldroyd-B models are considered due to the behavior of blood viscosity. In this paper, the effect of aneurysmatic artery on blood flow with permeability in human organs has been investigated. The non-Newtonian models have been applied to study the blood velocity, pressure, and wall shear stress in an aneurysmatic artery. A set of partial differential equations are transformed into dimensionless equations using non-dimensional variables and solved numerically. The novelty of this work is to identify the cardiovascular diseases in case of double aneurysmatic artery conditions for all models. The effect of wall shear stress is a vital factor to determine fatal arterial diseases which may be reported in the research center. The findings of this study can be used to know the atherosclerosis diseases and increase the understanding level of the double aneurysmal artery with the presence of permeability for which may help to enhance the knowledge of medical science. We have focused our consideration on the simulation of blood velocity and pressure in terms of blood flow rate for various Weissenberg numbers (Wi) and Peclet numbers (Pe). In this study, significant changes in blood velocity, pressure, and wall shear stress for all cases due to the presence of permeability at aneurysm in the artery are found. The effect of the Peclet number and Weissenberg number have played a key role in the blood flow at the porous area. The important effects on blood flow of aneurysmatic artery for blood velocity, pressure, and wall stress profiles are presented graphically for Newtonian and non-Newtonian models.

Keywords: Anuerysmatic artery; Oldroyd-B model; finite element method; permeability; viscoelasticity

NOMENCLATURE

σ	Stress Tensor (Pa)	μ_n	Polymer viscosity
σ_v	Viscous stress tensor (Pa)	μ_s	Solvent viscosity
σ_n	Solvent stress tensor (Pa)	V'	Anti-symmetry velocity gradient
L	height and the enclosure (m)	$\dot{\gamma}$	Rate of deformation tensor
I	Identity matrix	u, v	velocity components (ms^{-1})
Wi	Weissenberg number	U,V	Dimensionless velocity components
p	pressure (Nm^{-2})		**Greek symbols**
P	non-dimensional pressure	μ	Viscosity
Pe	Peclet number	γ	Deformation tensor
q	Flow rate (m^2/s)	ρ	density of the fluid (kgm^{-3})
λ_x	Relaxation time	υ	kinematic viscosity of the fluid (m^2s^{-1})
λ_d	Retardation time	$\boldsymbol{\tau}_s$	Extra-stress tensor
V	Symmetry velocity gradient		

1813-8235 (Print), 2070-8998 (Online) Received on: May 2021

1. Introduction

An aneurysm is defined as a dilatation of a blood vessel involving an increase in diameter above 50 percent compared with the expected normal diameter (Anand and Rajagopal, 2004). It is a result of an irregular growth or weakened blood vessel wall which is bubble or balloon shaped. Aortic aneurysm, Cerebral aneurysm, and Peripheral aneurysm are commonly found in the human body. The main reason and nature of aneurysms are still a vital subject of debate and almost 75 % of patients with aneurysms die before reaching the hospital. It may be 90 percent if we count prehospital deaths of ruptured aneurysm diseases (Cronenwett et al., 1985, Ingoldby et al., 1986). The study of blood flow has attracted many medical researchers, bioengineers etc. over the past years, due to its significant effect on several human cardiovascular diseases such as Arteriosclerosis, Bleeding, Stroke, kidney damage, and high blood pressure. The hemodynamical features of blood can change the rheological properties during the blood circulation system. It plays an important role in the expansion and progression of various cardiovascular diseases (Tu and Deville, 1996). A segment of the artery expands to form various aneurysms due to the vessel wall losing its structural integrity and continuously striking the pulsatile intraluminal pressure. Subsequently, the tension on its wall increases obeying Laplace's law and wall thickness plays a role in the expansion and ultimate rupture of an aneurysm and has shown that the stress in the arterial wall is inversely proportional to the wall thickness (Johansen, 1982). It is observed that with the increases of aneurysms the wall thickness has decreased. It is also found that the elasticity of the vessel wall has reduced with increasing age.

In case of the aneurysm and cardiovascular diseases the blood circulation is restricted and creates disorder in the blood flow system. As a result, blood flow loses its natural behavior and becomes non-Newtonian fluid. Currently, A good number of researchers (Keslerova and Karel, 2015, Bluth et al., 1990) have studied aneurysms from various perspectives and still have a great possibility to contribute to the sector. It is very important to determine the main factors that are the core responsibilities of the growth aneurysm and rupture. The aneurysm study of blood flow is very vital to understanding the blood behavior through enlarge tube as the wall shear stress, pressure decline and velocity development are some important factors to identify arterial diseases (Caro et al, 1971, Ernst, 1983, Friedman et al., 1992, Oka, 1973). The study of viscoelastic behavior of blood have been done (Thurston, 1973) which shows a relation between shear rate and viscoelasticity of blood. It has been studied of pulsatile blood flow in aneurysm and found the existence of vortex (Wille, 1981). The primary and secondary vortices are found (Fukushima et al.,1986) and shown that negative shear stressed the value and pressure fluctuation are remarkable in the aneurysm. An aneurysm is examined for the steady flow with the range of Reynold number from 500 to 2600 (Budwig, et al, 1993). The correlation between fluid dynamics and blood platelet deposition is found (Bluestein, et al, 1996) for steady flow in the aneurysm model. A numerical forecast of blood flow patterns and hemodynamic stresses have been studied in an abdominal aortic aneurysm in a two-aneurysm of different sizes (Finol and Amon, 2001). A data assimilation method (Elia et al, 2011) is used to show the numerical simulation of blood flow in 2D idealized stenosis with wall shear stress effect for capturing the shear-thinning rheological behavior. A numerical simulation is studied for the generalized Newtonian and Oldroyd-B model with an extended computation domain (Prokop and Kozel, 2013). The simulations of blood flow have improved by incorporating known data (Telma et al, 2014). An analysis has been done for viscous and viscoelastic fluids through the branching channel (Kumar and Naidu, 1995). A lot of study of aneurysm hemodynamics have been done for steady blood flow (Bernsdorf and Wang, 2009, Budwig et al, 1993) and shown the effect of the recirculating vortex on the aneurysm artery. It has been investigated (Mukhopadhyay and Layek, 2011) that the systematic analysis of blood flow in the presence of hematocrit at local aneurysm. In a dilated arterial vessel, the pulsatile suspension flow of blood with hemodynamics properties has been studied (Prasad et al, 2014). A thermodynamic framework is used to describe the viscoelastic response (blood) of bodies with multiple configurations (Rajagopal and Srinivasa, 2011). It has also discussed (Prasad et al.,2014) the steady flow of Jeffrey fluid through a tube for stenosis and aneurysm. A study of blood flow through an artery with overlapping stenosis has been done (Prasad et al., 2017). It is estimated of wall shear stress for thoracic aortic aneurysm and shown that the tools are very helpful for treatment methodology at arterial disease (Febina et al., 2018). The effect of cyclic stretch on vascular endothelial cells and abdominal aortic aneurysm (AAA) have been studied (Ramella et al., 2019) and shown that significant change in AAA is found due to wall calcification.

Recently, it is found (Parth et al., 2020) that the human lung system has been affected by biological and other factors for airflow and particle transport in arteries. They have shown that the velocity magnitude of airflow at the stenosis area is higher than in healthy airways. A study has been done (Pokhrel et al., 2020) that the pressure drop of the blood flow in the artery decreases with the increase of stenosis. An analysis of blood flow through aneurysm models have been discussed (Hong et al. 2020) and found out the hemodynamics trend of blood flow is affected by the various shape of the aneurysmal artery. Computational analysis has been completed (Shen, 2021) on the rupture of the cerebral aneurysm of blood flow and indicates that the angle of the arriving blood is significantly effective in the risky section on the aneurysmal artery wall. It has been studied (Rahman et al., 2021) that the transportation of nanoscale and microscale particles having realistic lung models with and without stenosis numerically. They have shown that with the increase of flow rate and the particle diameter, the particle deposition efficiency in airways has increased.

With the above inspiration, an effort is made in the present theoretical analysis to develop a mathematical model in order to study an aneurysmatic artery on blood flow in presence of permeability in human organs. A generalized cross model is used for non-Newtonian blood flow in this case. It is found (Muraki, 1983) that the mural thrombi and aneurysm rupture occurs in the enlarged area of the aneurysm. This study is one of the major physiological significance and more focus is also paid to show the major changes in the presence of partial permeable and permeable aneurysmal arterial wall for considered model.

In the present work, a numerical study of blood flow with aneurysmal artery has been studied to explore the effects of blood vessel swelling, the intensity of aneurysm, the wall shear stress, the dimensionless numbers, and the nonlinearity for Newtonian, Oldroyd-B and their generalized cases. A comprehensive scientific study is shown through their simulation of blood flow and graphical presentation for all cases. A comparison is shown with the previous result for validation of this study. The mathematical equations of blood flow are considered for the 2D steady case and then a finite element model has been developed for the present problem.

2. Mathematical Formulation

The swelled blood vessel portion having a double aneurysm within its artery is modeled and steady two-dimensional viscoelastic fluid in the existence of permeability with incompressible non-Newtonian fluid characterized by generalized cross model. Figure 1 is the main enthusiasm for considering the present model and the considered model in the present study is displayed in Figure 1. It is assumed that the blood fluid is uniformly injected or removed with speed V_0 at the aneurysmal artery and the parabolic velocity profile at the inlet is considered. The wall is rigid, and deformability is ignored due to the complexity of the constitutive equations. A mathematical model of the arterial segment has been used (Srivastava and Shailesh, 2010) for the overlapping stenosed model. The modified mathematical structure of the geometrical model with the presence of a double aneurysm is shown in Figure 2.

$$h_a = \frac{R(x)}{R_0(x)}$$

$$= \begin{cases} 1 + \dfrac{\varepsilon}{2R_0 l_a^4}\{11(x-l_0)\,l_a^3 - 47(x-l_0)^2\,l_a^2 + 72(x-l_0)^3 l_a - 36(x-l_0)^4\}, \; l_0 \le x \le l_0 + l_a \\ 1, \;\; otherwise \end{cases} \quad (1)$$

Where denotes the radius of the aneurysmatic section, $R_0(x)$ is the radius of the non-aneurysmatic area, l_a indicates the length of the aneurysm, and l_0 is the aneurysm location, ε is the maximum height of the aneurysm. The aneurysm positions are at x $= l_0 + \frac{l_a}{6}$ and $x = l_0 + \frac{5l_a}{6}$ respectively. The critical height is taken as $\frac{3\varepsilon}{4}$ at $x = l_0 + \frac{l_a}{2}$, from the origin.

.

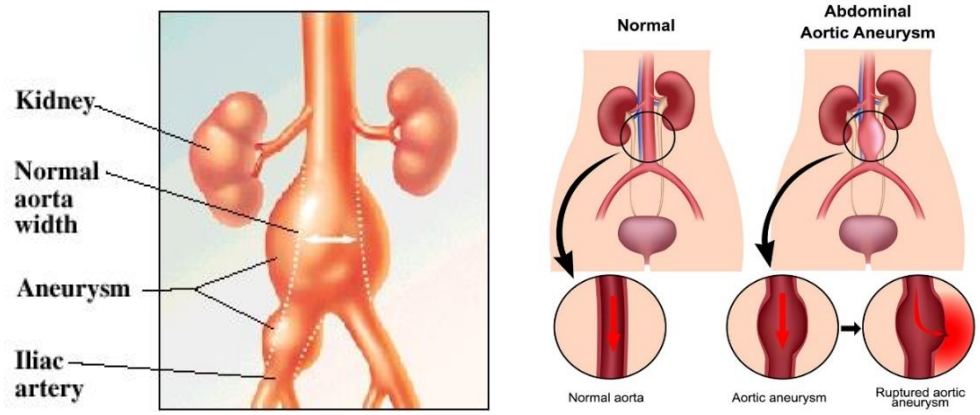

Figure 1. View of double aneurysmal (Mount Nittany Health, 2020) and rupture aneurysm (Health Direct,2020)

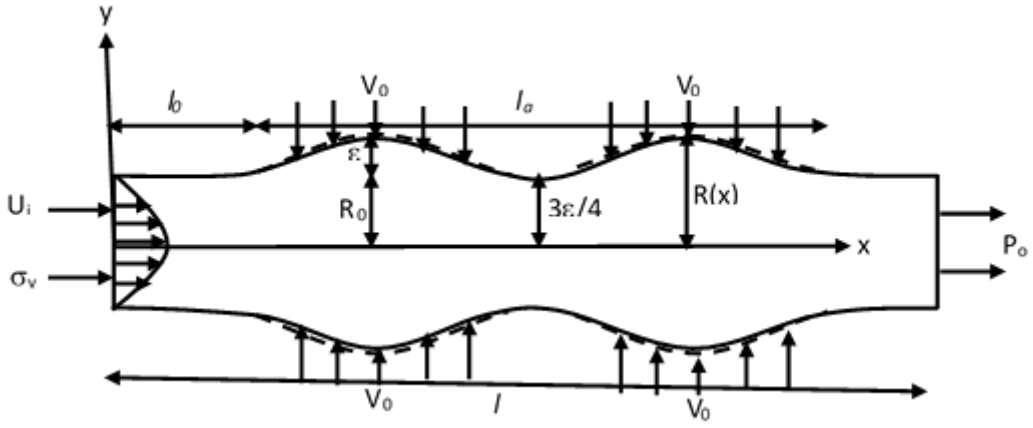

Figure 2. Aneurysmal geometric model

3. Mathematical model

Consider the blood flow in the enlarge artery to be two-dimensional, steady, symmetric and fully developed. The flowing blood is the properties of viscoelastic and shear-thinning where the generalized cross model is used. In vector form, the basic mathematical equations of the continuity equation, Navier Stokes equation (Bird et al., 2001, Faveroa et al., 2010) and Oldroyd-B constitutive equation (Owens and Phillips, 2002) for steady-state blood flow are as follows:

Continuity Equation

$$\nabla . \boldsymbol{u} = 0 \tag{2}$$

Momentum Equation

$$\rho \frac{\partial \boldsymbol{u}}{\partial t} + \rho(\boldsymbol{u}.\nabla)\boldsymbol{u} = -\nabla p + \mu_n \Delta \boldsymbol{u} + \nabla . \boldsymbol{\sigma} + \rho \boldsymbol{f} \tag{3}$$

Oldroyd-B constitutive equation:

$$\boldsymbol{\sigma} + \lambda_x [\frac{\partial \boldsymbol{\sigma}}{\partial t} + (\boldsymbol{u}.\nabla)\boldsymbol{\sigma}] = 2\mu_v \boldsymbol{V}(u) + \lambda_x [\boldsymbol{\sigma V}^{/} - \boldsymbol{V}^{/}\boldsymbol{\sigma} - \boldsymbol{\sigma V} - \boldsymbol{V\sigma}] \tag{4}$$

Here $\boldsymbol{u}$ is the velocity vector, $\boldsymbol{u}= (u_1, u_2, u_3)^T$, ρ is the constant density, $\boldsymbol{\sigma}$ is the extra stress tensor, μ is dynamic viscosity, λ_x the relaxation and the symmetric part of the velocity gradient, $V = \frac{1}{2}(\nabla \boldsymbol{u} + \nabla \boldsymbol{u}^T)$

i.e. $\boldsymbol{\sigma} = 2\mu \boldsymbol{V}$.

The following dimensionless variables are introduced to normalized equations (2) to (4).

$x=LX,\ t = Lt^*/U,\ \mathbf{u} = \mathbf{U}U_0,\ \boldsymbol{\sigma} = U\mu\boldsymbol{\sigma}/L$ (5)

$p = \mu UP/L,\ f = F\mu U/L^2,\ \nabla = \nabla/L$ (6)

$Wi = \lambda_x U/L,\ Pe = UL/\alpha = Re\ Sc,\ Sc = \mu/\rho L,$ (7)

Using dimensionless scale equations (5-7), the governing non-dimensional blood flow equations are obtained for steady state 2D aneurysm vessel in domain Ω as follows:

Continuity Equation

$$\nabla . \boldsymbol{U} = 0 \tag{8}$$

Momentum Equation

$$\frac{Pe}{Sc}[(\boldsymbol{U}.\nabla)\boldsymbol{U}] = -\nabla p + (1-\lambda)\Delta \boldsymbol{U} + \nabla . \boldsymbol{\sigma} + \mathbf{F} \tag{9}$$

Oldroyd-B constitutive equation:

$$W_i[(\boldsymbol{U}.\nabla)\boldsymbol{\sigma}] + \boldsymbol{\sigma} = 2\mu_v \mathbf{V}(\mathbf{U}) + W_i[(\nabla \boldsymbol{U})]\boldsymbol{\sigma} + \boldsymbol{\sigma}\,(\nabla \boldsymbol{U})^t \tag{10}$$

The total viscosity are composed of Newtonian viscosity (solvent, μ_n) and viscoelasticity (polymer, μ_v) components, $\mu = \mu_n + \mu_v$ and the relation between relaxation (λ_x) and retardation time (λ_d),is $\frac{\lambda_d}{\lambda_x} = \frac{\mu_n}{\mu_n + \mu_v}$. The extra-stress tensor, $\boldsymbol{\sigma} = \boldsymbol{\sigma}_n + \boldsymbol{\sigma}_v$, where Newtonian part, $\boldsymbol{\sigma}_n = 2\mu_n \mathbf{V}$ and viscoelastic part, $\boldsymbol{\sigma}_v + \lambda_x \frac{\partial \boldsymbol{\sigma}_v}{\partial t} = 2\mu_v \mathbf{V}$. Reynolds number (*Re*), Pectlet number (*Pe*) and Weissenberg number (*Wi*) are dimensionless numbers. In the case of shear-thinning behaviors of blood flow, the shear rate dependent viscosity function $\mu(\dot{\gamma})$ and the generalized Cross model (Sequeira et al. 2007, Galdi et al. 2008) given by

$$\mu(\dot{\gamma}) = \mu_\infty + \frac{\mu_0 - \mu_\infty}{(1+(\lambda\dot{\gamma})^b)^a} \tag{11}$$

with the parameters a, b, λ>0. On the basis of blood shear-thinning (μ_n) and viscoelasticity (σ_v) properties, we have four models such as (i) Newtonian ($\mu_n = \mu_\infty$ = constant, σ_v =0) (ii) Generalized Newtonian ($\mu_n = \mu(\dot{\gamma})$,$\sigma_v$ =0) (iii) Oldroyd-B ($\mu_n = \mu_\infty$ = constant, σ_v) (iv) Generalized Oldroyd-B ($\mu_n = \mu(\dot{\gamma})$,$\sigma_v$).

It is required to prescribe either Dirichlet (velocity) or Neumann (surface force) boundary conditions (Prokop and Kozel, 2013) at the inlet to develop parabolic velocity profile due to insufficient physiological data.

The mathematical parabolic velocity profile and the corresponding extra stresses components (Bodnar et. Al. 2011) are as follows

$$\mathbf{u} = 1.5\, U_i(1-y^2);\ 0 \le y \le 2,\ \mathbf{v} = 0 \tag{12}$$

$$\sigma_{11} = 2\mu_v \mathrm{Wi}\left(\frac{\partial u}{\partial y}\right)^2, \sigma_{12} = \mu_v \frac{\partial u}{\partial y},\ \boldsymbol{\sigma}_{22} = 0 \tag{13}$$

At outlet, pressure value is constant, and no slip conditions is appropriate at vessel walls. Due to pressure force (P_o) the stress is acting at the boundary

$$\boldsymbol{\sigma}.\,\mathbf{n} = -\,P_o\,\mathbf{n}$$

For permeability, the constant velocity (v_0) is used at first aneurysm. In case of Oldroyd-B and its generalized model, the extra stresses components are used at inlet and others boundary conditions remain same as Newtonian and generalized Newtonian. On the walls, no slip conditions are used for the velocity together with the condition for the normal component of the extra stress: $\mathbf{u} = 0$ and $(\boldsymbol{\sigma}.\,\mathbf{n}).\,\mathbf{n} = 0$, Where $\mathbf{n}$ is the boundary unit normal vector.

In this research work, the continuity equation (2), momentum equation (3) and Oldroyd-B equation (4) are considered to account for the blood viscoelasticity. The following models (Bodnar et. Al. 2011) are tested and shown in Table 1 for different flow rates (q = 0.05, 0.1, 2 cm^3/ s), that correspond to the common blood flow rates in human body for the combination of shear-thinning and viscoelasticity.

Table 1: Models outline

Name of Model	Shear-thinning (μ_n)	Viscoelasticity ($\boldsymbol{\sigma}_v$)
Newtonian	$\mu_n = \mu_\infty$= constant	$\boldsymbol{\sigma}_v = 0$
Generalized Newtonian	$\mu_n = \mu(\dot{\gamma})$	$\boldsymbol{\sigma}_v = 0$
Oldroyd-B	$\mu_n = \mu_\infty$= constant	$\boldsymbol{\sigma}_v$
Generalized Oldroyd-B	$\mu_n = \mu(\dot{\gamma})$	$\boldsymbol{\sigma}_v$

4. Numerical Approximations

The partial differential equations subjected to the boundary conditions simultaneously have been solved for the dependent variables such as velocity, pressure and stress tensor. The numerical procedure of the finite element method (Dechaumphai, 1999, Taylor and Hood, 1973) has been used to solve this problem and details are given below. The velocity and viscoelasticity Equations (8-10) result in a set of non-linear coupled equations for which an iterative scheme is adopted. To ensure convergence of the numerical algorithm the following criteria are applied to all dependent variables over the solution domain

$$\sum \left|\psi_{ij}^{n} - \psi_{ij}^{n-1}\right| \leq 10^{-5}$$

Where, Ψ represents a dependent variable u, p,σ; the indexes i, j indicates a grid point; and the index n is the current iteration at the grid level. The six-node triangular element is used in this work for the development of the finite element equations. All six nodes are associated with velocities as well as stress tensor; only the corner nodes are associated with pressure. This means that a lower order polynomial is chosen for pressure, and it is satisfied through continuity equation. The velocity component and the stress tensor distributions and linear interpolation for the pressure distribution according to their highest derivative orders in the differential Equations (8-10) are defined as follows.

$$u(X,Y) = N_\alpha u_\alpha,\ \sigma(X,Y) = N_\alpha \sigma_\alpha,\ p(X,Y) = H_\lambda p_\lambda \qquad (11)$$

Where, α = 1, 2,…, …, 6; λ= 1, 2, 3; N_α are the element interpolation functions for the velocity components and the stress tensor, and H_λ are the element interpolation functions for the pressure.

To derive the finite element equations, the method of weighted residuals is applied to the continuity equation (8), the momentum Equations (9) and the viscoelasticity Equation (10), we get.

$$\int_A N_\alpha(\nabla.\boldsymbol{u})\,dA = 0 \tag{12}$$

$$\frac{Pe}{Sc}\int_A N_\alpha(\boldsymbol{u}.\nabla)\boldsymbol{u}\;)dA = -\int_A H_\lambda\,\nabla p\,dA + \int_A N_\alpha(\nabla.\boldsymbol{\sigma})\,dA + (1-\lambda)\int_A N_\alpha\,\Delta\boldsymbol{u}\,dA + \int_A N_\alpha f\,dA \tag{13}$$

$$W_i\int_A N_\alpha(\boldsymbol{u}.\nabla)\,\sigma\,dA + \int_A N_\alpha\sigma\,dA = 2\int_A \mu_v\,N_\alpha \boldsymbol{V}(u)\,dA + W_i\int_A N_\alpha\big((\nabla\boldsymbol{u})\sigma + \sigma^t(\nabla\boldsymbol{u})\big)\,dA \tag{14}$$

Where, A is the element area. Gauss's theorem is then applied to Equations (12-14) to generate the boundary integral terms associated with the surface tractions and extra stress tensor. Then Equations (13-14) become,

$$\frac{Pe}{Sc}\int_A N_\alpha(\boldsymbol{u}.\nabla)\boldsymbol{u}\;)dA + \int_A H_\lambda\,\nabla p\,dA - \int_A N_\alpha(\nabla.\boldsymbol{\sigma})dA - (1-\lambda)\int_A N_\alpha\,\Delta\boldsymbol{u}\,dA - \int_A N_\alpha f\,dA = \int_{s_0} N_\alpha S_x\,ds_0 \tag{15}$$

$$W_i\int_A N_\alpha(\boldsymbol{u}.\nabla)\,\sigma\,dA + \int_A N_\alpha\sigma\,dA - 2\int_A \mu_v\,N_\alpha\boldsymbol{V}(u)\,dA - W_i\int_A N_\alpha\big((\nabla\boldsymbol{u})\sigma + \sigma^t(\nabla\boldsymbol{u})\big)\,dA = \int_A N_\alpha\sigma_w\,ds_w \tag{16}$$

Here Equations (15) specify surface tractions (S_x, S_y) along outflow boundary S_0 and Equation (16) specifies velocity components and stress tensor that can be applied from domain along wall boundary S_w. Substituting the element velocity component distributions, the stress tensor distribution, and the pressure distribution from Equations (8-10) the finite element equations can be written in the form,

$$K_{\alpha\beta}{}^x u_\beta + K_{\alpha\beta}{}^y v_\beta = 0 \tag{17}$$

$$(K_{\alpha\beta\gamma}{}^x u_\beta u_\gamma + K_{\alpha\beta\gamma}{}^y v_\beta u_\gamma) + M_{\alpha\mu}{}^x P\mu + K_{\alpha\beta}{}^x\sigma_\beta + K_{\alpha\beta}{}^y\sigma_\beta$$
$$+(1-\lambda)(S_{\alpha\beta}{}^{xx} + S_{\alpha\beta}{}^{yy})u_\beta - f_x K_\alpha = Q_\alpha{}^u \tag{18}$$

$$W_i(K_{\alpha\beta\gamma}{}^x\,u_\beta\sigma_\gamma + K_{\alpha\beta\gamma}{}^y v_\beta\sigma_\gamma) + K_{\alpha\beta}\sigma_\mu - \mu_v(K_{\alpha\beta}{}^x u_\alpha + K_{\alpha\beta}{}^y u_\beta)$$
$$-W_i\big(K_{\alpha\beta\gamma}{}^x u_\beta\sigma_\gamma + K_{\alpha\beta\gamma}{}^y u_\beta\sigma_\gamma\big) = Q_\alpha{}^T \tag{19}$$

Where, the coefficients in element matrices are in the form of the integrals over the element area and along the element edges S_0 and S_w as,

$$K_{\alpha\beta}{}^x = \int_A N_\alpha N_{\beta,x}dA,\; K_{\alpha\beta}{}^y = \int_A N_\alpha N_{\beta,y}dA,\; K_{\alpha\beta\gamma}{}^x = \int_A N_\alpha N_\beta N_{\gamma,x}dA,$$
$$K_{\alpha\beta\gamma}{}^y = \int_A N_\alpha N_\beta N_{\gamma,y}dA,\; K_{\alpha\beta} = \int_A N_\alpha N_\beta dA,\; S_{\alpha\beta}{}^{xx} = \int_A N_{\alpha,x} N_{\beta,x}dA,\; S_{\alpha\beta}{}^{yy} = \int_A N_{\alpha,y} N_{\beta,y}dA,$$

$$M_{\alpha\mu}{}^x = \int_A H_\alpha H_{\mu,x}dA,\; M_{\alpha\mu}{}^y = \int_A H_\alpha H_{\mu,y}dA,\; Q_\alpha{}^u = \int_{S_0} N_\alpha S_x dS_0,\; Q_\alpha{}^T = \int_{S_0} N_\alpha\sigma_w dS_w$$

These element matrices are evaluated in closed-form ready for numerical analysis. Details of the derivation for these element matrices are omitted herein for brevity (Reddy, 1993; Zeinkiewicz, 1971; Roy and Basak, 2005).

The derived finite element equations, Equations (17-19), are nonlinear. These nonlinear algebraic equations are solved by applying the Newton-Raphson iteration technique by first writing the unbalanced values from the set of the finite element Equations (17-19) as

$$F_{\alpha^p} = K_{\alpha\beta^x} u_\beta + K_{\alpha\beta^y} v_\beta$$

$$F_{\alpha^u} = Re(K_{\alpha\beta\gamma^x}\, u_\beta u_\gamma + K_{\alpha\beta\gamma^y}\, v_\beta u_\gamma) + M_{\alpha\mu^x} P\mu - K_{\alpha\beta^x}\sigma_\beta - K_{\alpha\beta^y}\sigma_\beta + (1-\lambda)(S_{\alpha\beta^{xx}} + S_{\alpha\beta^{yy}})u_\beta - f_x K_\alpha - Q_{\alpha^u}$$

$$F_{\beta^\sigma} = W_i(K_{\alpha\beta\gamma^x}\, u_\beta\sigma_\gamma + K_{\alpha\beta\gamma^y} v_\beta\sigma_\gamma) + K_{\alpha\beta}\sigma_\beta - \mu_v(K_{\alpha\beta^x}\, u_\beta + K_{\alpha\beta^y}\, v_\beta) - 2W_i\left(K_{\alpha\beta\gamma^x}\, u_\gamma\sigma_\beta + K_{\alpha\beta\gamma^y}\, u_\gamma\sigma_\beta\right) - Q_{\alpha^\sigma}$$

This leads to a set of algebraic equations with the incremental unknowns of the element nodal velocity components, temperatures, and pressures in the form,

$$\begin{bmatrix} K_{uu} & K_{u\sigma} & K_{up} \\ K_{\sigma u} & K_{\sigma\sigma} & 0 \\ K_{pu} & 0 & 0 \end{bmatrix} \begin{Bmatrix} \Delta u \\ \Delta\sigma \\ \Delta p \end{Bmatrix} = - \begin{Bmatrix} F_\alpha{}^u \\ F_\alpha{}^\sigma \\ F_\beta{}^p \end{Bmatrix} \tag{20}$$

Where, $K_{uu} = Re(K_{\alpha\beta\gamma^x} U_\gamma + K_{\alpha\gamma\beta^x} U_\gamma + K_{\alpha\beta\gamma^y} V_\beta) + (1-\lambda)\left(S_{\alpha\beta^{xx}} + S_{\alpha\beta^{yy}}\right)$

$K_{u\sigma} = -K_{\alpha\beta^x} {}_{-K_{\alpha\beta^y}} U\gamma$, $K_{up} = M_{\alpha\mu^x}$,

$K_{\sigma u} = W_i K_{\alpha\beta\gamma^x}\sigma_c - K_{\alpha\beta^x}\mu_v$, $K_{\sigma\sigma} = K_{\alpha\beta} - 2W_i(K_{\alpha\beta\gamma^x} U_c + K_{\alpha\beta\gamma^y} U_c)$

$K_{\sigma p} = 0, K_{pu} = K_{\alpha\beta^x}, K_{p\rho} = 0 = K_{pp}$.

The iteration process is terminated if the percentage of the overall change compared to the previous iteration is less than the specified value. To solve the sets of the global nonlinear algebraic equations in the form of matrix, the Newton-Raphson iteration technique has been adapted through PDE solver (COMSOL MULTIPHYSIS, 2013) and MATLAB programing (Kumar et al., 2010).

5. Numerical Results

The aim of this mathematical model is to know and bring out the effects of permeable anuerysmatic artery, wall shear stress, and dimensionless numbers on blood flow for the models of (i) Newtonian (μ_n = constant, $\boldsymbol{\sigma}_v$ =0) (ii) Generalized Newtonian (μ_n = $\mu(\dot{\gamma}), \boldsymbol{\sigma}_v = 0$) (iii) Oldroyd-B ($\mu_n$ = constant, $\boldsymbol{\sigma}_v$) (iv) Generalized Oldroyd-B (μ_n = $\mu(\dot{\gamma}), \boldsymbol{\sigma}_v$ .The Newtonian (N), generalized Newtonian (GN), Oldroyd-B (OD) and generalized Oldroyd-B (GD) models are used to study the influence of the shear-thinning and viscoelastic behavior of blood. In this work, we are concerned with non-Newtonian fluids type, with the flows of incompressible viscoelastic Oldroyd-B fluids. It is very important to select the blood viscosity for accuracy in blood flow simulations. In 2D aneurysm case, the generalized Cross model, the mathematical parabolic velocity profile and the corresponding extra stresses components are used for shear-thinning properties of blood.

A validation test has done (Prokop and Kozel, 2013) to evaluate the accuracy of the numerical simulation and flow visualization for Newtonian (N), generalized Newtonian (GN), Oldroyd-B (OD) and generalized Oldroyd-B (GD) cases. It has computed blood velocity, pressure and wall shear stress with dimensionless numbers *Wi* and *Pe* for considered model. For this numerical study, the following blood properties are considered: $0 \le Wi \le 1$, $0 < Pe \le 1000$, $\mu_0 = 0.16$ Pa.s, $\mu_n = 0.0036$ Pa.s, a = 1.23,b = 0.64, λ = 8.2s, ρ = 1050 kg.m-3, l_0 = 2R, l= 10R, R= 3.1mm, and l_a = 6R.

The purpose of this paper is to discuss the effects of the permeable aneurysmatic artery, wall shear stress and dimensionless numbers on blood flow for all cases to study the influence of hemodynamic variables. The simulation of blood flows in terms of axial velocity contour lines have shown in Figure 3 as follows.

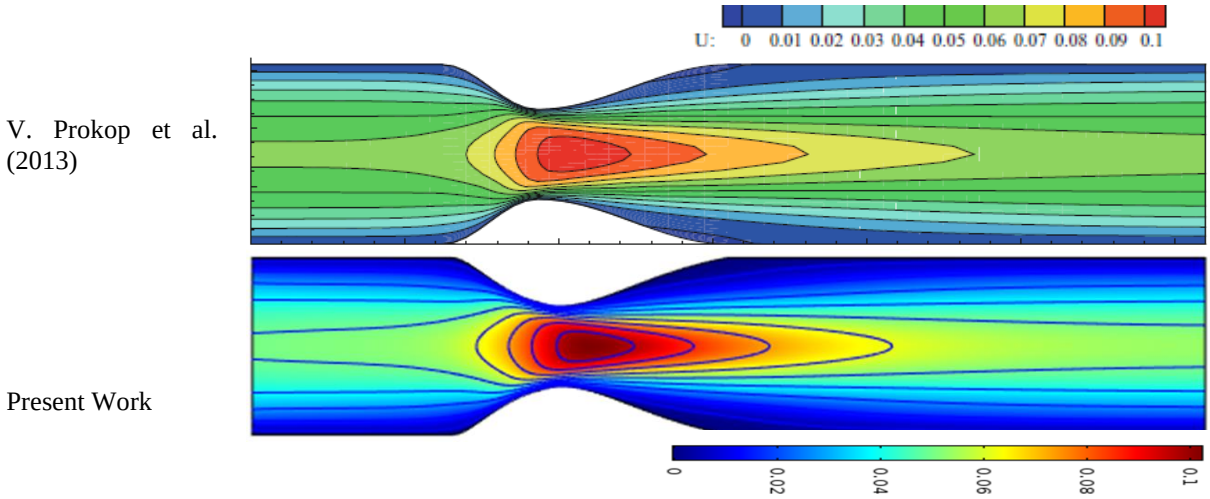

Figure 3: Comparison of velocity contour of blood flow through stenosis artery

5.1 Aneurysmal vessel effects on blood flow field

The velocity contour lines have provided a detailed description of the blood flow field and it is a specific interest of the model. The velocity profiles of blood flow of the four different models Newtonian, Generalized Newtonian, Oldroyd-B, Generalized Oldroyd-B are presented in Figures 4-6 with constant flow rate. It is very interesting that the only recirculation zones are originated in generalized Oldroyd-B model and absent at rest of the models for simple aneurysm (no permeability) blood vessel. At permeable aneurysm, some permanent recirculation zones are found between the aneurysms. It is noted that the recirculation zones are migrating toward the proximal end of the aneurysm cavity and adjacent to vessel wall for all models. These recirculation zones are symbolic of regions over a significant portion of each model where the flow is separated. At generalized Newtonian and Oldroyd-B model the recirculation zones have shrunk considerably. Because of, a shear-thinning viscosity of blood which leads to the increase of the local viscosity in the low-shear regions.

In Figure 4, the flow separation regions are initiated at the beginning of both aneurysm and blood flow patterns are symmetric along vessel axis. But in the case of permeable boundary conditions at Figures 5 and 6, the flow separation regions are created at the bottom section of first aneurysm but different in second aneurysm and the blood flow patterns are migrating towards upper vessel wall.

The graphical presentation of velocity profiles is shown in Figure 7 for all four models at dimensionless number Wi=0.6 and Pe=1000 with absent of permeable, partial permeable and both permeable aneurysms. From the Figure 7a, the minimum value of velocity is found in second enlargement regions and peak value is at outlet for Newtonian and Oldroyd-B case. Due to permeability, the velocity has increased and provide highest velocity at generalized models in Figures 7a & 7b. In Figures 7a, 7b, and 7c, the minimum values are found at aneurysm for all cases and the lowest value is approximately 0.044 which is in the 2nd aneurysm for the Oldroyd-B model at the permeable aneurysm. It is a very interesting finding that the blood flow patterns are almost the same for impermeable and permeable case, but the lowest value is found for generalized models in presence of permeability. In the presence of porosity at aneurysm, the blood velocity is more affected for Oldroyd-B fluid. In the case of partial porosity at aneurysm, the lowest value is observed at the Oldroyd-B and generalized Oldroyd-B cases. The difference of blood velocities is 0.014 and 0.019, and the deviation of velocity is almost 22.22% for partially permeable aneurysms and 30.15% for both permeable aneurysms respectively. On the other hand, the maximum values are 0.069, 0.065, and 0.061 for impermeability, partial permeability, and both permeability aneurysm respectively. The maximum changes of blood velocity are 24.29% (approx.) for the Oldroyd-B model whereas 11.59% for the generalized Oldroyd-B. So, the effect of permeability aneurysm artery on the blood flow is more prominent for the generalized Oldroyd-B case. In the recirculation zone, the blood shear-thinning behavior is remarkable and local viscosity increases significantly. The viscoelastic effects may become more important for other cases.

Newtonian

Generalized Newtonian

Oldroyd-B

Generalized Oldroyd-B

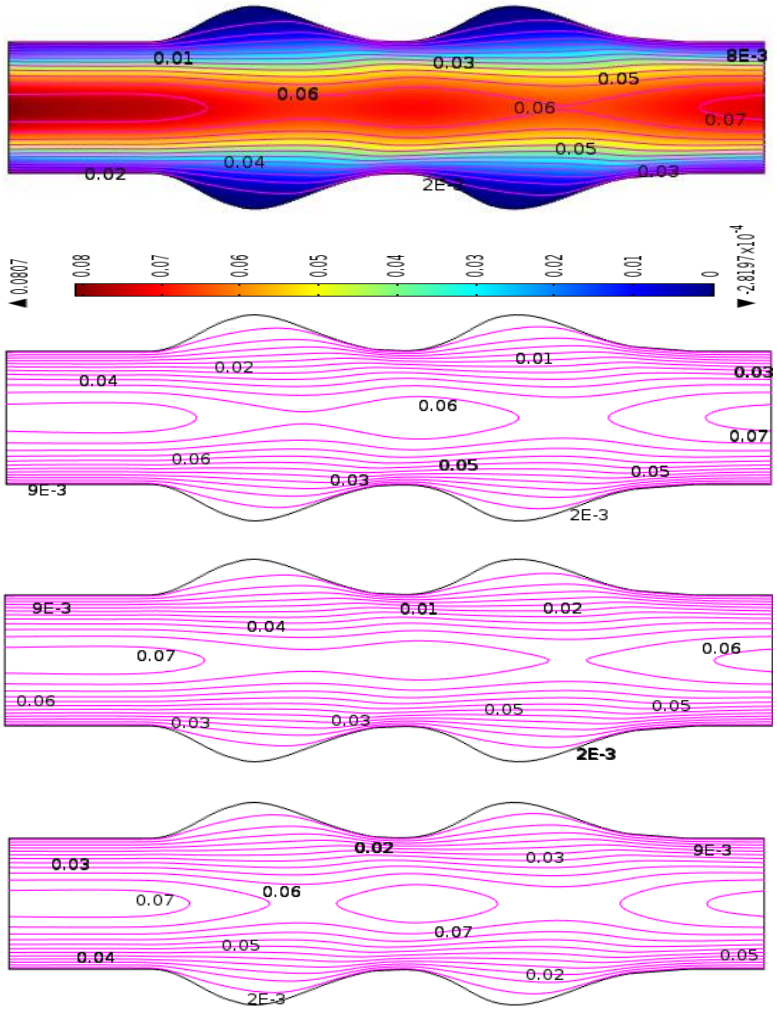

Figure 4: Velocity contour line on blood flow through anuerysmatic blood vessel at *Pe*=1000 and *Wi* = 0.6

Newtonian

Generalized Newtonian

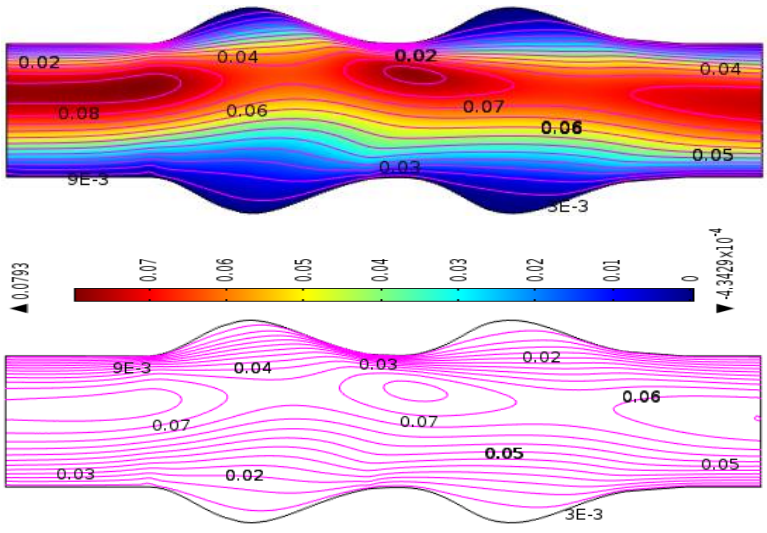

Oldroyd-B

Generalized Oldroyd-B

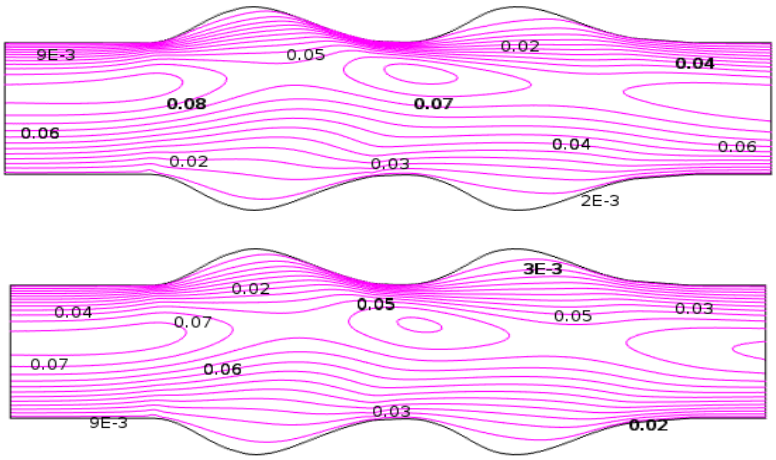

Figure 5: Velocity contour line on blood flow through partial permeable anuerysmatic blood vessel at *Pe*=1000 and *Wi* = 0.6

Newtonian

Generalized Newtonian

Oldroyd-B

Generalized Oldroyd-B

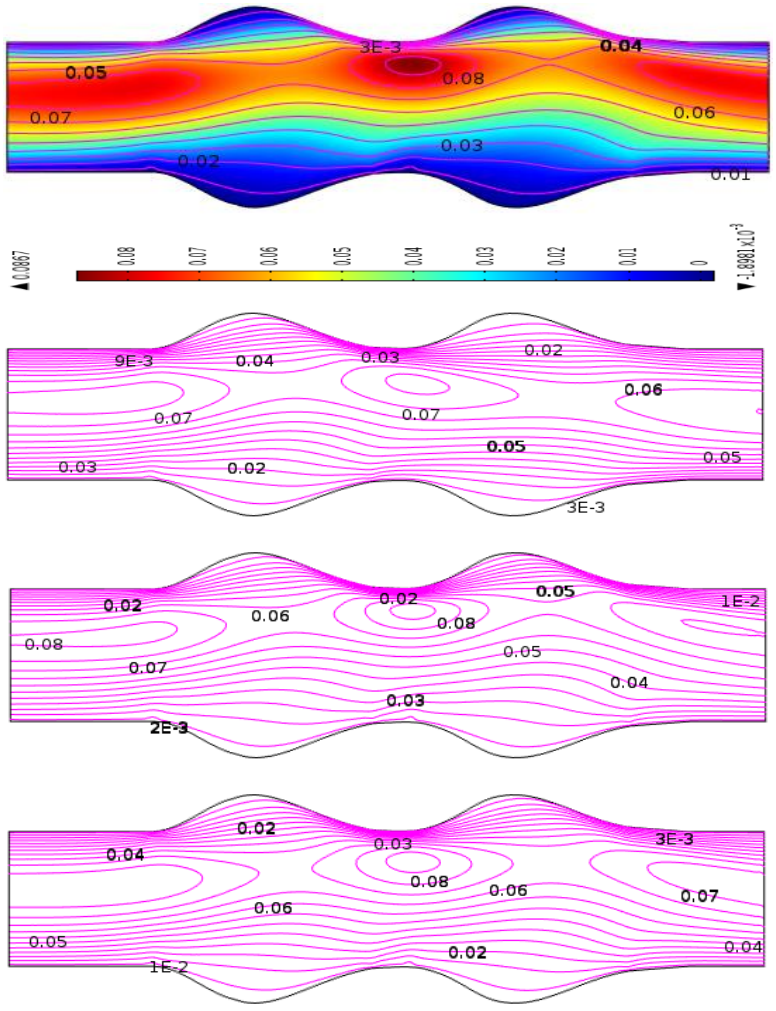

Figure 6: Velocity distribution on blood flow through permeable anuerysmatic blood vessel at *Pe*=1000 and *Wi* = 0.6

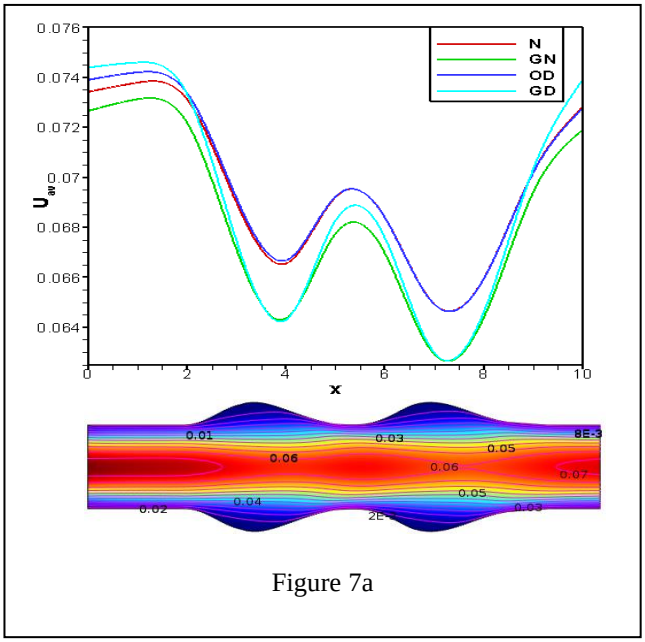

Figure 7a

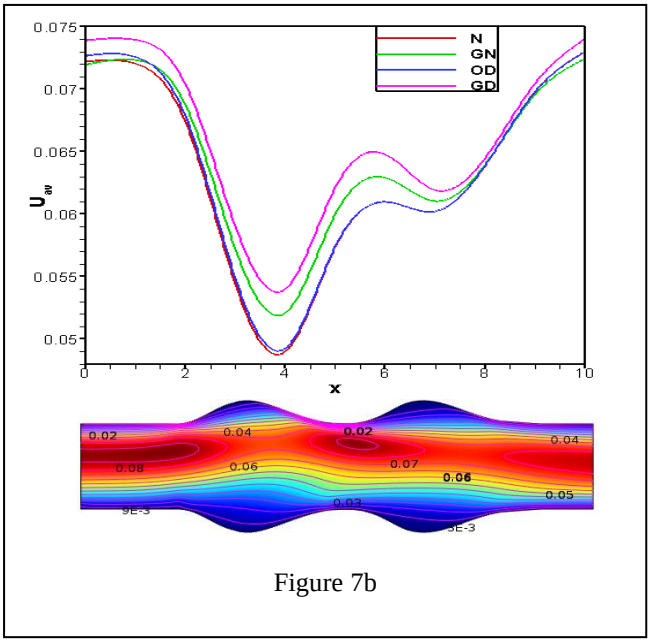

Figure 7b

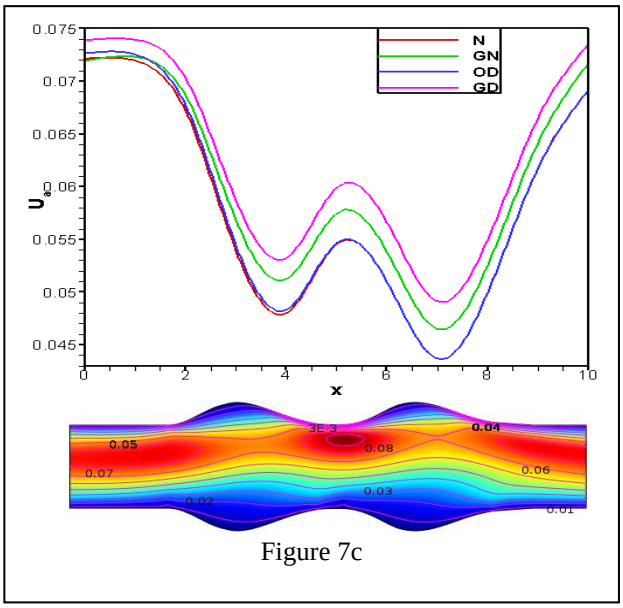

Figure 7c

Figure 7: Velocity profile without permeable (Figure 7a), partial permeable (Figure 7b) and both permeable (Figure 7c) aneurysm along vessel when Pe=1000 and Wi=0.6.

5.2 Aneurysmal vessel effects on pressure distribution

The blood flow simulation of pressure circulation is present in terms of contour plot for all models in Figures 8, 9 and 10 with permeability and without permeability of aneurysm. At Figure 8, the iso-pressure contours show the way to gain a minimum value at the separation point and decreased mechanically. The maximum value has peaked at the reattachment point, which created a stagnation point, and fell suddenly at the beginning of first aneurysm. Due to presence of permeability, the pressure has decreased rapidly and gained minimum value at outlet in Figure 10. The flow separation points, and stagnation point have migrated towards upper blood vessel wall. The patterns of pressure distribution have changed magnificently along aneurysm for porosity of vessel wall and pressure contour lines converted from steep to slant gradually at second aneurysm. The pressure gradient is very intensive at the end of second aneurysm, and it is varied substantially throughout the blood vessel. The contour of blood pressure results indicates that twice aneurysms are formed, the blood flow has

increased the blood pressure at dilating area. The significant changes occur in blood pressure at first dilating (aneurysm) because of penetrable vessel wall. At generalized Oldroyd-B model, the pressure is more dominated compared to others due to the shear-thinning behavior of blood viscosity.

The numerical graph of pressure profiles is shown in Figure 11 for all four models at Wi=0.6 and Pe=1000. From Figures 11a, 11b, and 11c, the least pressure values are almost -1.8, -2.2, -2.9 at the outlet for impermeability, partial permeability, and both permeability aneurysm respectively in the case of the generalized Oldroyd-B model. The maximum pressure changes are 61.11% in the presence of permeability aneurysm for generalized Oldroyd-B case and almost 22.22% for Oldroyd-B case. In the middle of the aneurysm, the highest changes of blood pressure are found for the generalized Oldroyd-B case. It is observed that the maximum pressures are 0.8, 0.7, and 0.65 for Newtonian fluid for all cases. The blood pressure has changed 18.75% at most for both permeable aneurysm arteries. At Figure 11, the minimum pressure is originated after second dilating for all models. The lowest value is found at Oldroyd-B model due to porosity at Figure 11c which leads to non-Newtonian fluid flow is faster than Newtonian fluid.

Newtonian

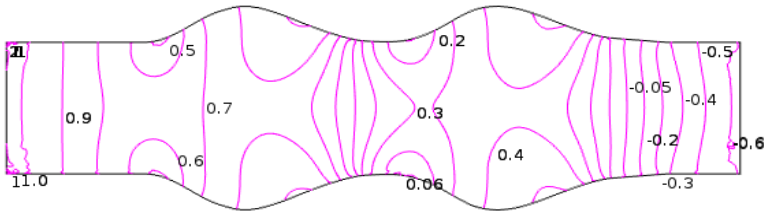

Generalized Newtonian

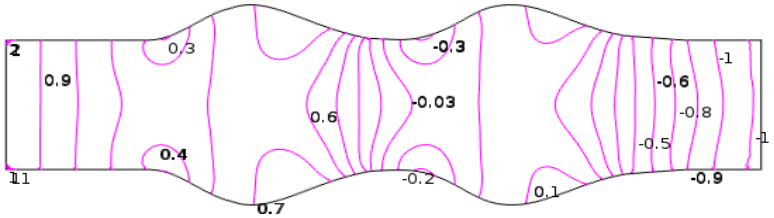

Oldroyd-B

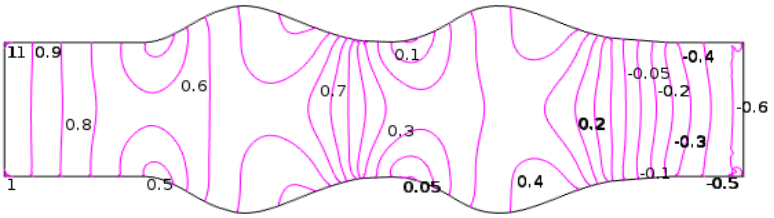

Generalized Oldroyd-B

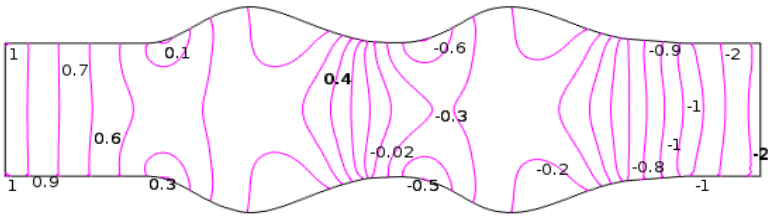

Figure 8: Pressure distribution on blood flow through anuerysmatic (without permeable) blood vessel at *Pe*=1000 and *Wi* = 0.6

Newtonian

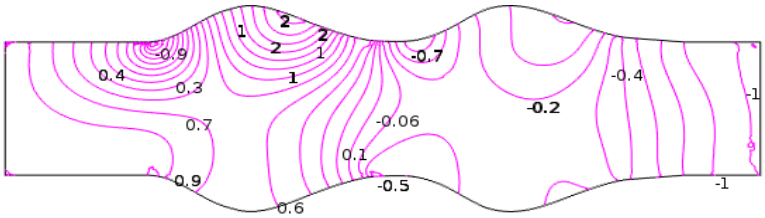

Generalized Newtonian

Oldroyd-B

Generalized Oldroyd-B

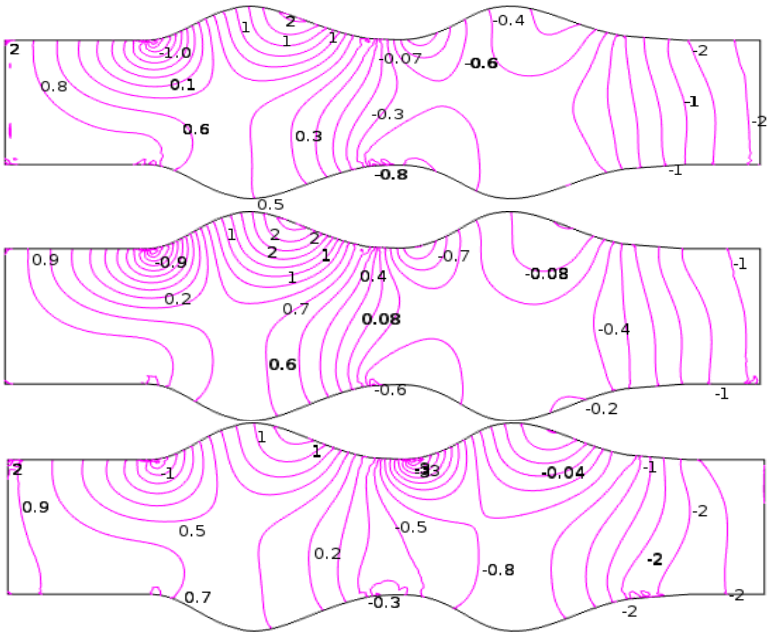

Figure 9: Pressure distribution on blood flow through partial permeable anuerysmatic blood vessel at *Pe*=1000 and *Wi* = 0.6

Newtonian

Generalized Newtonian

Oldroyd-B

Generalized Oldroyd-B

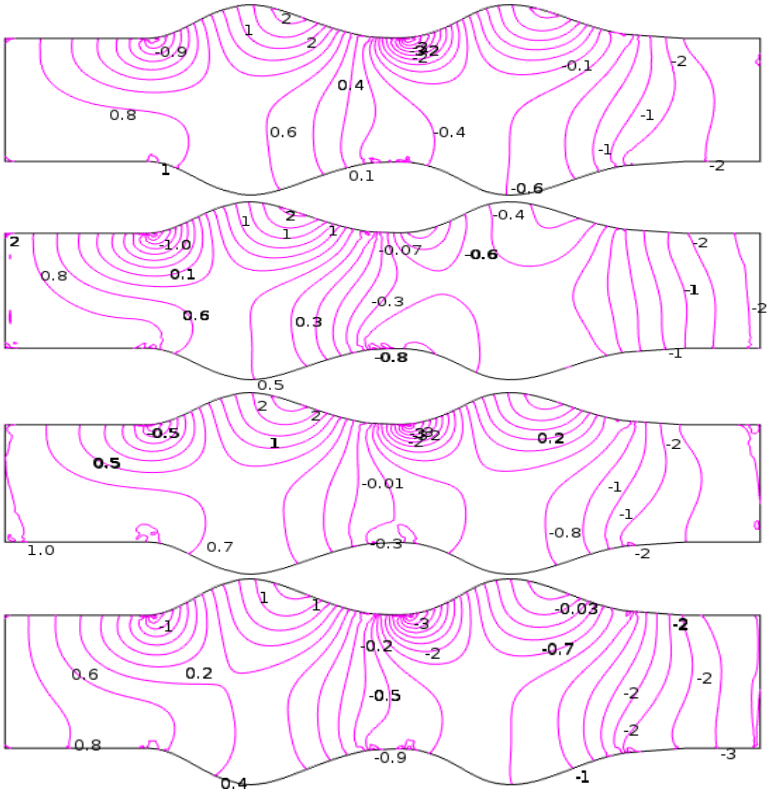

Figure 10: Pressure distribution on blood flow through permeable anuerysmatic blood vessel at *Pe*=100 and *Wi* = 0.6

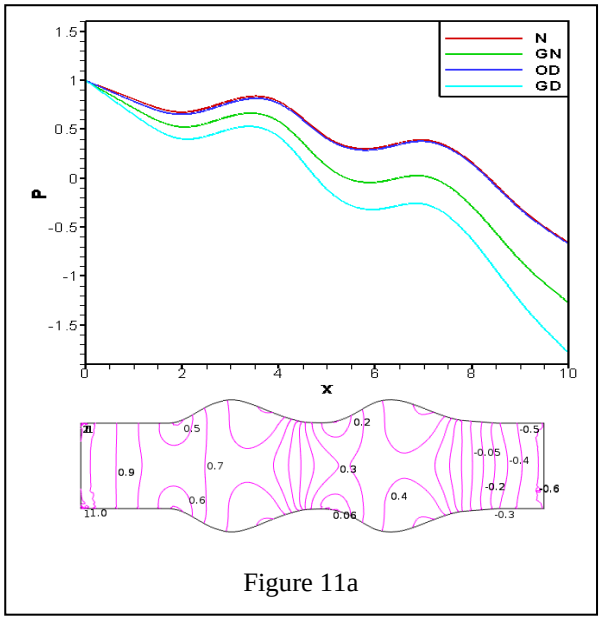

Figure 11a

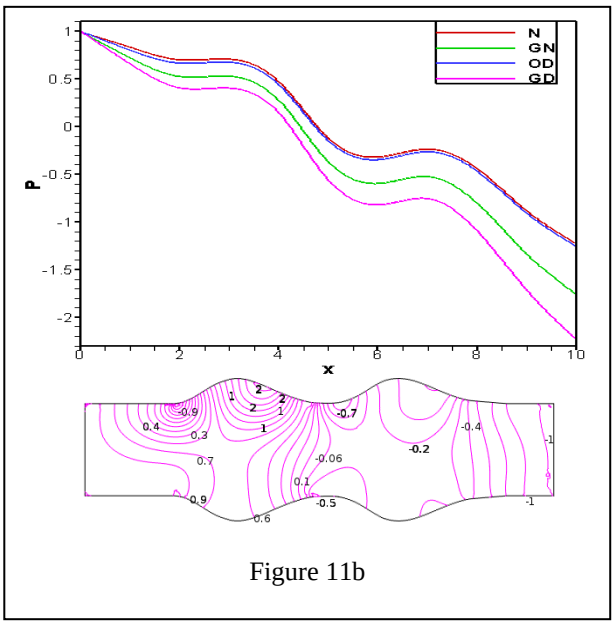

Figure 11b

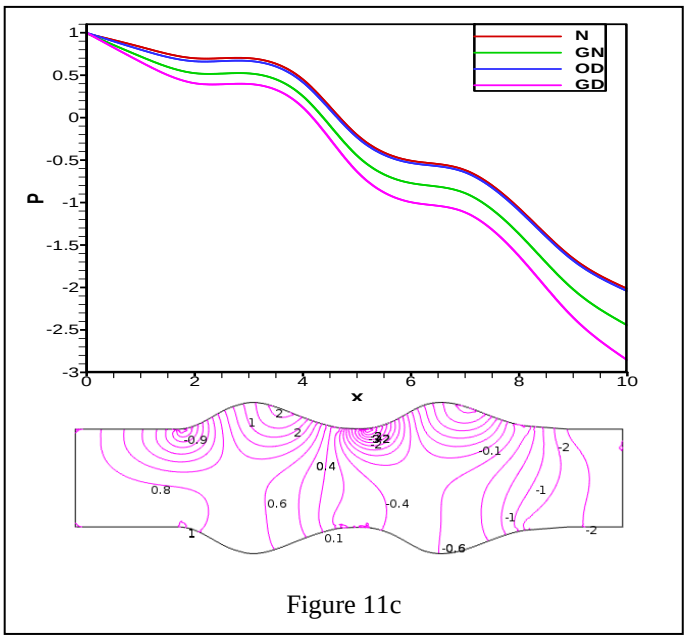

Figure 11c

Figure 11: Pressure profile with no permeable (Figure 11a), partial permeable (Figure 11b) and both permeable (Figure 11c) aneurysm along vessel when Pe=1000 and Wi=0.6.

5.3 Wall Shear Stress effects on Blood flow

The wall shear stress (wss) effects on blood flow are an important factor to identify the fatal cardiovascular diseases in the arteries. The impact of wss of blood flow has shown at Figures 12 for Newtonian model with impermeable and permeable aneurysm at constant flow rate. The surface force has worked tangentially at blood vessel artery, acting against the fluid flow and a vital parameter in blood flow simulation. In Figure12, the wss profiles are shown at Pe=1000 and Wi =0.6 for all cases. The profiles have displayed the oscillation of wall shear stress on blood flow along vessel axis for all models. The maximum value is found at inlet and then it is going down rapidly at the genesis of permeable aneurysm for all models. It speeds up dramatically at first aneurysm and suddenly fall down for all models. The lowest value is found just after permeable aneurysm in the

case of Newtonian fluid. We have observed that the wss of generalized Newtonian and Oldroyd-B model is marginally higher than the others model and the wall shear stress of generalized Oldroyd-B model is significantly higher than other models.

The comparable graphical study of impermeable and permeable aneurysm for the wss are shown in Figure 13 with various Wi = 0.0, 0.5 and 1.0. At Wi = 0.0, the wss is greater in the case of impermeable aneurysm because of viscous effect on blood flow. The influence of porosity aneurysm the wss is lower at Wi=0.0 in Newtonian case. From the Figures. 13, it is clear that the wall shear stresses have a significant change due to permeability.

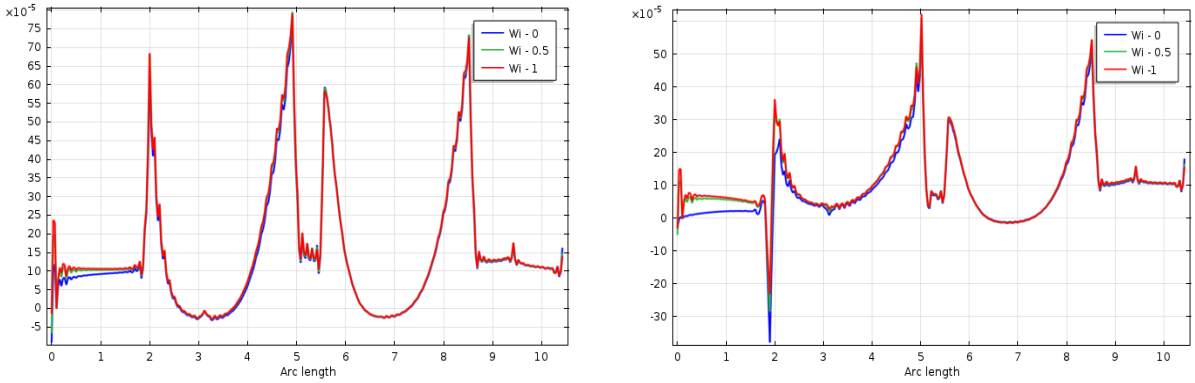

Figure 12: Effects of wall shear stress on blood flow through impermeable (left) and permeable (right) aneurysmal artery for Newtonian case at Pe=1000 and Wi = 0.6.

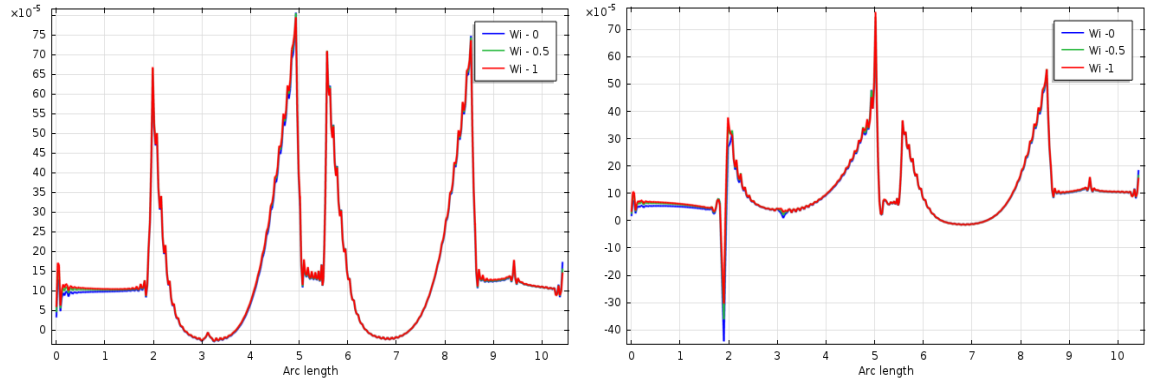

Figure 13: Effects of wall shear stress on blood flow through impermeable (left) and permeable (right) aneurysm for different Wi at Oldroyd-B Model case with Pe=1000.

6. Conclusion

The finite element method is used to simulate the blood flow through permeable aneurysm artery. The generalized Newtonian model, Oldroyd-B models and generalized Oldroyd-B models are used for non-Newtonian fluid blood viscosity. Due to shear-thinning and blood viscosity, Oldroyd-B type models play important role to find out blood flow variables. The numerical study is performed to analyze the blood flow patterns through permeable aneurysm in steady flow for all cases. The outcomes of blood flow characteristics and wall shear stress are correlated to blood viscoelasticity. The blood flow variables are foremost and decreased for all models along vessel axis at permeable aneurysm. The porosity aneurysm and blood viscosity are main factors for the Newtonian and Non-Newtonian solution. At the present problems, the numerical method is used to solve the governing equations seems to be sufficiently strong and effective for the appropriate resolution. To solve these nonlinear equations, the Newton-Raphson iteration method is used for solutions of the nodal velocity component, tensor component, and pressure by considering Weissenberg numbers of 0.0, 0.5 and 1.00 and Pectel numbers of 10^3 to 3×10^3.

The effect of an aneurysmal artery on blood flow in the presence of permeability in human organs has been studied for various values of relevant parameters. It is an important finding that non-Newtonian types model provide accurate result compare to Newtonian types model to study blood flow characteristics for permeable

aneurysm artery. Numerical models and simulation provide an effective non-invasive technique to obtain accurate data of blood flow in human artery and appropriate identification of arterial diseases. The following outcomes may be concluded from the present study:

- Significant changes of blood flow characteristics at permeable anuerysm for all four models are found in this investigation. The blood velocity has been reduced due to presence of permeability at aneurysm is another important finding.

- The effect of the blood flow on the wall shear stress is an important factor to determine fatal arterial diseases.

- The minimum value of blood velocity and maximum value of pressure are found at porous aneurysm. But in impermeable aneurysm, the lowest velocity has been found at second aneurysm for all cases.

- The effect of dimensionless numbers Peclet (Pe) and Weissenberg (Wi) are more striking at porous region and blood flow variables have been changed dramaticaly. The pressure distribution have been increased with increase of Pe at permeable aneurysm but pressure patterns have been decreased with the increase of Wi for generalized Oldroyd-B cases.

- The blood flow patterns are alike for impermeable and permeable aneurysm but the maximum variation of blood velocity and blood pressure has occurred for the generalized Oldroyd-B model.

- The impact of a permeable aneurysm on blood flow is another key factor to identify cardiovascular diseases.

- Elliptic types of recirculation zone are originated between the aneurysm regions for all four models and non-axisymmetric profiles are found at the entrance.

Acknowledgements

We are grateful to the Bangladesh University of Professionals (BUP) and Bangladesh University of Engineering and Technology (BUET) to provide all facilities during the work.

References

Anand, M. and Rajagopal, K. R. (2004): A shear-thinning viscoelastic fluid model for describing the flow of blood, International Journal of Cardiovascular Medicine and Science, Vol.4, No. 2, pp.59–68.

Bodnar, T., Sequeira, A., Prosi, M., (2011): On the shear-thinning and viscoelastic effects of blood ow under various flow rates, Applied Mathematics and Computation, Vol. 217(11), pp. 5055-5067. https://dx.doi.org/10.1016/j.amc.2010.07.054

Bird, R.B., Stewart, W.E. and Lightfoot, E.N. (2001). Transport Phenomena, 2th edition. John Wiley Sons. ISBN 0-471-41077-2.

Bernsdorf, J. and Wang, D. (2009): Non-Newtonian blood ow simulation in cerebral aneurysms, Computers and Mathematics with Applications, Vol. 58, No. 5, pp.1024-1029. https://dx.doi.org/10.1016/j.camwa.2009.02.019

Bluestein, D., Niu L, Schoephoerster R. T. and Dewanjee, M. K. (1996): Steady flow in an aneurysm model: correlation between fluid dynamics and blood platelet deposition, Journal of Biomechanical Engineering, 118, No. 3, pp. 280-286. https://dx.doi.org/10.1115/1.2796008

Bluth, E. I., Murphey, S. M., Hollier, L. H., and Sullivan, M. A. (1990): Color flow Doppler in the evaluation of aortic aneurysms, International Angiology**,** Vol. 9, No. 1 pp. 8-10.

Budwig RS., Elgar D., Hooper H. and Slippy J. (1993): Steady Flow in Abdominal Aortic Aneurysm Models, Journal of Biomechanical Engineering, Vol.115, No. 4A, pp. 418-423. https://dx.doi.org/10.1115/1.2895506

Caro, C. G., Fitzgerald, J. M. and Schroter, R. C. (1971): Atheroma and Wall Shear. Observation, Correlation and Proposal of a Shear Dependent Mass Transfer Mechanism for Atherogenesis, Proceedings of The Royal Society, Vol. 177, No. 1046, pp. 109-159. https://dx.doi.org/10.1098/rspb.1971.0019

COMSOL Multiphysics (2013): 4.3a users guide, Stockholm, Sweden.

Cronenwett J L, Murphy TF, Zelenock GB, Whitehouse WM Jr, Lindenauer SM, Graham LM, Quint LE, Silver TM and Stanley JC (1985): Actuarial analysis of variables associated with rupture of small abdominal aortic aneurysms, Surgery, Vol. 98, No. 3, pp. 472–83.
Dechaumphai P. (1999): Finite Element Method in Engineering, Chulalongkorn University Press, Bangkok.
Galdi G. P., Rannacher R., A. Robertson M., Turek S. (2008): Hemodynamical flows, modeling, analysis and simulation, Birkhauser Verlag AG, Basel Switzerland. https://dx.doi.org/10.1007/978-3-7643-7806-6
Elia M D, Perego M. and Veneziani A (2011): A variational data assimilation procedure for the incompressible Navier-Stokes equations in hemodynamics, Journal of Scientific Computing, Vol. 52, pp. 340-359.
Ernst, C. B (1993): Abdominal aortic aneurysm, The New England Journal of Medicine, Vol. 328, No. 16, pp.1167-72. https://dx.doi.org/10.1056/NEJM199304223281607
Faveroa J.L., Secchi A.R. , Cardozoa N.S.M., Jasakc H. (2010): Viscoelastic flow analysis using the software OpenFOAM and differential constitutive equations, Journal of Non-Newtonian Fluid Mechanics, Vol. 165, PP.1625–1636. doi: https://dx.doi.org/10.1016/j.jnnfm.2010.08.010
Febina J, Yacin M S and Sudharsan N M (2018): Wall shear stress estimation of thoracic aortic aneurysm using computational fluid dynamics, Computational and Mathematical Methods in Medicine, Vol. 2018, pp.1-12. https://dx.doi.org/10.1155/2018/7126532.
Finol Ender A. and Amon, C. H. (2001): Blood flow in abdominal aortic aneurysms: pulsatile flow hemodynamics, Journal of Biomechanical Engineering, Vol. 123, No.5, pp. 474-484. https://dx.doi.org/10.1115/1.1395573
Friedman, M. H., Bargeron, C. B., Duncan, D. D., Hutchins, G. M., and Mark, F. F.(1992): Effects of arterial compliance and non-Newtonian rehology on correlation between intimal thickness and wall shear, ASME Journal of Biomechanical Engineering, Vol. 109, No.3, pp, 317-320. https://dx.doi.org/10.1115/1.2891389
Fukushima, T., Matszuzawa, T., and Homma, T. (1986): Visualization and finite element analysis of pulsatile flow in models of abdominal aortic aneurysm, Biorehology, Vol. 26, No.2, pp. 109-130. https://dx.doi.org/10.3233/bir-1989-26203
Health Direct (2020): Aortic aneurysm, https://healthdirect.gov.au/aortic-aneurysm (accessed May 15, 2020).
Hong, L. S., Adib, M. A. H. M., Matalif, M. U., Abdullah M. S., Taib N. H. M., Hassan R. (2020): Modeling and simulation of blood flow analysis on simplified aneurysm models, International Conference on Technology, Engineering and Sciences (ICTES), Vol. 917, 012067, https://dx.doi.org/10.1088/1757-899X/917/1/012067
Ingoldby, C. J. H., Wujanto, R. and Mitchell, J.E. (1986): Impact of Vascular Surgery on Community Mortality from Ruptured Aortic Aneurysms, The British Journal of Surgery. Vol. 73, No. 7, pp. 551-563. https://dx.doi.org/10.1002/bjs.1800730711
Johansen, K. H. (1982): Aneurysms, Scientific American, Vol. 247, No. 1, pp. 110-125. https://dx.doi.org/10.1038/scientificamerican0782-110
Keslerova, R. and Karel, K. (2015): Numerical modelling of viscous and viscoelastic fluids flow through the branching channel, Programs and Algorithms of Numerical Mathematics 17, Institute of Mathematics AS CR, Prague, pp. 100-105. https://dx.doi.org/10.1007/978-3-319-05591-6_66
Kumar, B.V.R. and Naidu, K.B. (1995): Finite element analysis of nonlinear pulsatile suspension flow dynamics in blood vessels with aneurysm, Computers in Biology Medicine, Vol. 25, No.1, pp.1-20. https://dx.doi.org/10.1016/0010-4825(95)98881-d
Kumar, B. R., Kumar, G.A. and Kumar, S.M. (2010): MATLAB^{R} and its Application in Engineering. Panjab University, India.
Mount Nittany Health (2020): Abdominal Aortic Aneurysm Stable, https://mountnittay.org/articles/healthsheets/37754 (accessed May 15, 2020).
Mukhopadhyay, S. and Layek, G.C. (2011): Analysis of blood flow through a modeled artery with an aneurysm, Applied Mathematics and Computation, Vol. 217, No.16, pp. 6792-6801. https://dx.doi.org/10.1016/j.amc.2010.10.011
Muraki, N. (1983): Ultrasonic studies of the abdominal aorta with special reference to hemodynamic considerations on thrombus formation in the abdominal aortic aneurysm, Journal of Japanese College Angiology, Vol. 23, pp. 401-413.
Oka, S. (1973): Pressure development in a non-Newtonian flow through a tapered tube, Biorheology, Vol. 10, No. 2, pp. 207–212. https://dx.doi.org/10.3233/bir-1973-10213
Owens, R. G., Phillips T. N. (2002): Computational Rheology, Imperial College Press. https://dx.doi.org/10.1142/p160
Prasad, K.M., Vijaya, R.B. and Umadevi, C. (2015): Effects of stenosis and poststenotic dilatation on Jeffrey fluid flow in arteries, International Journal of Research in Engineering and Technology. Vol. 4, No. pp.13, pp.195-201. https://dx.doi.org/10.15623/IJRET.2015.0413032

Prasad K.M., Sudha T. and Phanikumar M. V. (2017): Investigation of blood flow through an artery in the presence of overlapping stenosis, Journal of Naval Architecture and Marine Engineering. Vol. 14, No.1, pp. 39. https://dx.doi.org/10.3329/jname.v14i1.31165

Pokhrel P. R., Kafle J., Kattel P., Gaire H. P. (2020): Analysis of blood flow through artery with mild stenosis, Journal of Institute of Science and Technology, Vol. 25, No.2, pp.33-38.

Prokop V. and Kozel K (2013): Numerical simulation of Generalized Newtonian and Oldroyd-B Fluids, Computing, Vol. 95, pp. 587-597.

Rajagopal K.R. and Srinivasa A.R. (2011): A Gibbs-potential-based formulation for obtaining the response functions for a class of viscoelastic materials, Proceedings of The Royal Society, Vol. 467, No. 2125, pp. 39-58. https://dx.doi.org/10.1098/rspa.2010.0136

Rahmana Md. M, Zhaoa M., Islam M. S., Dongd K, Sahac S. C. (2021): Numerical study of nanoscale and microscale particle transport in realistic lung models with and without stenosis, International Journal of Multiphase Flow, Vol. 145, https://dx.doi.org/10.1016/j.ijmultiphaseflow.2021.103842

Ramella M., Bertozzi G., Fusaro, L., Talmon, M., Manfredi M., Catoria M. C., Casella F., Porta C. M., Boldorini R., Fresu L. G., Marengo E. and Boccafoschi F. (2019): Effect of cyclic stretch on vascular endothelial cells and abdominal aortic aneurysm (AAA): Role in the inflammatory response, International Journal of Molecular science, Vol. 20, No. 2, pp. 287. https://dx.doi.org/10.3390/ijms20020287

Reddy J.N. (1993): An Introduction to Finite Element Analysis, McGraw-Hill, New-York.

Roy S.,and Basak T. (2005): Finite element analysis of natural convection flows in a square cavity with nonuniformly heated wall(s), Int. J. Eng. Sci. 43 (2005) 668-680. Doi: https://dx.doi.org/10.1016/j.ijengsci.2005.01.002

Sequeira A., Janela J. (2007): An overview of some mathematical models of blood rheology, M.S.Pereira (ed.), A portrait of state-of-the-art research at the Technical University of Lisbon, Springer, PP. 65–87. https://dx.doi.org/10.1007/978-1-4020-5690-1_4

Shen X. Y., Gerdroodbary M. B., Poozesh A., Abazari A. M. and Imani S. M. (2021): Effects of blood flow characteristics on rupture of cerebral aneurysm: Computational study, International Journal of Modern Physics C, Vol. 32, No. 11, 2150143, https://dx.doi.org/10.1142/S0129183121501436

Singh P., Raghav V., Padhmashali V., Paul G., Islam M.S. and Saha S. C. (2020): Airflow and Particle Transport Prediction through Stenosis Airways, Int. J. Environ. Res. Public Health, Vol. 17, No. 3, PP. 1-19. https://dx.doi.org/10.3390/ijerph17031119

Srivastava,V.P. and Shailesh M. (2010): Non-Newtonian Arterial Blood Flow through an Overlapping Stenosis, Applications of Applied Mathematics: An International Journal, Vol. 5, No. 1, pp. 225 -238.

Taylor C. and Hood P. (1973): A Numerical Solution of the Navier-Stokes Equations Using Finite Element technique, Computer and Fluids, Vol. **1**, No. 1, pp.73-100. https://dx.doi.org/10.1016/0045-7930(73)90027-3

Telma G., Jorge T and Adelia S (2014): Optimal control in blood flow simulations, International Journal of Non-Linear Mechanics. Vol. 64, pp. 57-69. https://dx.doi.org/10.1016/J.IJNONLINMEC.2014.04.005

Thurston G.B. (1973): Frequency and shear rate dependence of viscoelasticity of blood, Biorheology, Vol. 10, No. 3, pp. 375-381. https://dx.doi.org/10.3233/bir-1973-10311

Tu C. and Deville M. (1996): Pulsatile flow of non-Newtonian fluids through arterial stenoses, Journal of Biomechanics, Vol. 29, No. 7, pp. 899–908. https://dx.doi.org/10.1016/0021-9290(95)00151-4

Wille, S.O.(1981): Pulsating pressure and flow in an arterial aneurysm simulated in a mathematical model, Journal of Biomedical Engineering, Vol. 3, No. 2, pp.153-158. https://dx.doi.org/10.1016/0141-5425(81)90010-8

Zeinkiewicz O.C.,Taylor R.L., and Too J.M., (1971), Reduced integration technique in general analysis of plates and shells, Int. J. Numer. Methods Eng. (3) 275-290. https://dx.doi.org/10.1002/nme.1620030211